AD-A038 685 STANFORD RESEARCH INST MENLO PARK CALIF F/G 11/2
CHARACTERIZATION OF THE DYNAMIC BEHAVIOR OF POROUS SOLIDS. VOLU--ETC(U)
MAR 76 D A SHOCKEY, M J GINSBERG, J P WILHELM DNA001-74-C-0150
UNCLASSIFIED DNA-3961F-7 NL

1 OF 1
AD
A038685

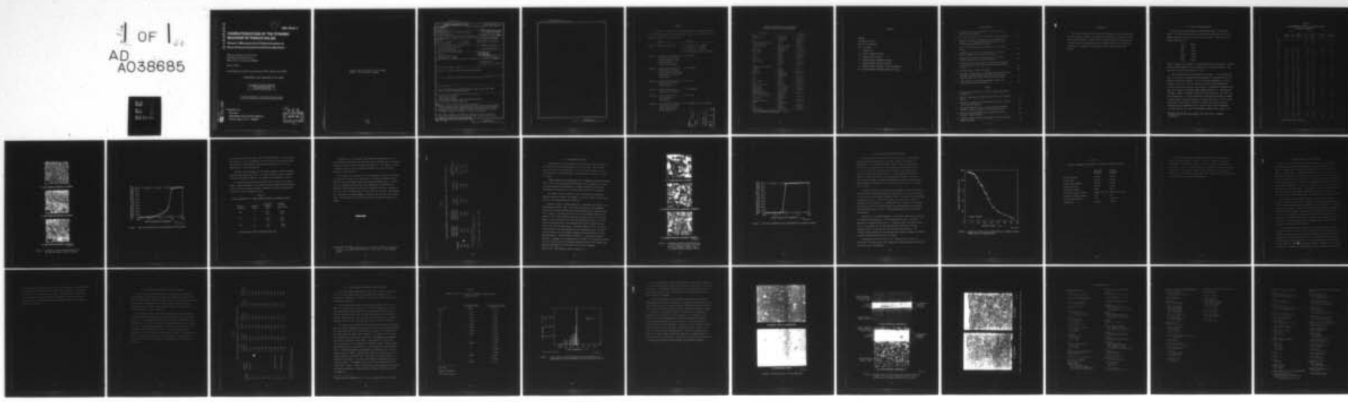

END
DATE
FILMED
5-77

(12)

DNA 3961F-7

CHARACTERIZATION OF THE DYNAMIC BEHAVIOR OF POROUS SOLIDS

Volume 7-Microstructural Characterization of Several Porous Ceramics and Porous Beryllium

Stanford Research Institute
333 Ravenswood Avenue
Menlo Park, California 94025

March 1976

Final Report for Period 14 January 1974—31 January 1976

CONTRACT No. DNA 001-74-C-0150

APPROVED FOR PUBLIC RELEASE;
DISTRIBUTION UNLIMITED.

THIS WORK SPONSORED BY THE DEFENSE NUCLEAR AGENCY
UNDER RDT&E RMSS CODE B342076464 N99QAXAC30840 H2590D.

Prepared for
Director
DEFENSE NUCLEAR AGENCY
Washington, D. C. 20305

Destroy this report when it is no longer needed. Do not return to sender.

UNCLASSIFIED

SECURITY CLASSIFICATION OF THIS PAGE (When Data Entered)

REPORT DOCUMENTATION PAGE

READ INSTRUCTIONS BEFORE COMPLETING FORM

1. REPORT NUMBER DNA 3961F-7	2. GOVT ACCESSION NO.
3. RECIPIENT'S CATALOG NUMBER	
4. TITLE (and Subtitle) CHARACTERIZATION OF THE DYNAMIC BEHAVIOR OF POROUS SOLIDS. Volume 7 - Microstructural Characterization of Several Porous Ceramics and Porous Beryllium.	5. TYPE OF REPORT & PERIOD COVERED Final Report for Period 14 Jan 74—31 Jan 76
	6. PERFORMING ORG. REPORT NUMBER SRI Project PYU-3163
7. AUTHOR(s) Donald A. Shockey, J. P. Wilhelm, M. J. Ginsberg, D. R. Curran	8. CONTRACT OR GRANT NUMBER(s) DNA 001-74-C-0150
9. PERFORMING ORGANIZATION NAME AND ADDRESS Stanford Research Institute 333 Ravenswood Avenue Menlo Park, California 94025	10. PROGRAM ELEMENT, PROJECT, TASK AREA & WORK UNIT NUMBERS Subtask N99QAXAC308-40
11. CONTROLLING OFFICE NAME AND ADDRESS Director Defense Nuclear Agency Washington, D.C. 20305	12. REPORT DATE March 1976
	13. NUMBER OF PAGES 38
14. MONITORING AGENCY NAME & ADDRESS(if different from Controlling Office)	15. SECURITY CLASS (of this report) UNCLASSIFIED
	15a. DECLASSIFICATION/DOWNGRADING SCHEDULE

16. DISTRIBUTION STATEMENT (of this Report)

Approved for public release; distribution unlimited.

332 500

17. DISTRIBUTION STATEMENT (of the abstract entered in Block 20, if different from Report)

18. SUPPLEMENTARY NOTES

This work sponsored by the Defense Nuclear Agency under RDT&E RMSS Code B342076464 N99QAXAC30840 H2590D.

19. KEY WORDS (Continue on reverse side if necessary and identify by block number)

Sintered Porous Alumina
Flame Sprayed Alumina
Plasma Sprayed Alumina Titanate and Hafnium Titanate
Plasma Sprayed Distended Beryllium

20. ABSTRACT (Continue on reverse side if necessary and identify by block number)

Porous sintered alumina, flame sprayed alumina, plasma sprayed aluminum titanate, plasma sprayed hafnium titanate, and plasma sprayed distended beryllium were used in the high explosive, gas gun and electron beam experiments reported in Volumes 4, 5 and 6 in this series.

This report, Volume 7, describes the fabrication process, the microstructural characteristics, and the important chemical, physical and mechanical properties of each material.

DD FORM 1 JAN 73 1473 EDITION OF 1 NOV 65 IS OBSOLETE

UNCLASSIFIED

SECURITY CLASSIFICATION OF THIS PAGE (When Data Entered)

UNCLASSIFIED

SECURITY CLASSIFICATION OF THIS PAGE(*When Data Entered*)

UNCLASSIFIED

SECURITY CLASSIFICATION OF THIS PAGE(*When Data Entered*)

PREFACE

This report is Volume 7 in a seven-part series on Characterization of the Dynamic Behavior of Porous Solids. The titles and authors of the individual reports in the series are:

	Title	Authors
Volume 1.	Summary of Results	D. R. Curran, R. E. Tokheim, M. J. Ginsberg, L. Seaman, A. B. Lutze, D. C. Erlich, J. T. Rosenberg, and D. A. Shockey
Volume 2.	Computational Models for Predicting the Dynamic Stress Response of Some Porous Ceramics in a Radiation Environment	R. E. Tokheim
Volume 3.	Computational Model for Predicting the Dynamic Stress Response of Porous Beryllium in a Radiation Environment	R. E. Tokheim
Volume 4.	Electron Beam Studies of Porous Beryllium and Porous Ceramics	A. B. Lutze
Volume 5.	Dynamic Response of Beryllium--Experiments	J. T. Rosenberg
Volume 6.	Dynamic Response of Porous Ceramics--Experiments	D. C. Erlich
Volume 7.	Microstructural Characterization of Several Porous Ceramics and Porous Beryllium	D. A. Shockey and J. P. Wilhelm

Conversion factors for U.S. customary to metric (SI) units of measurement.

To Convert From	To	Multiply By
angstrom	meters (m)	1.000 000 X E -10
atmosphere (normal)	kilo pascal (kPa)	1.013 25 X E +2
bar	kilo pascal (kPa)	1.000 000 X E +2
barn	meter^2 (m^2)	1.000 000 X E -28
British thermal unit (thermochemical)	joule (J)	1.054 350 X E +3
calorie (thermochemical)	joule (J)	4.184 000
cal (thermochemical)/cm^2	mega joule/m^2 (MJ/m^2)	4.184 000 X E -2
curie	*giga becquerel (GBq)	3.700 000 X E +1
degree (angle)	radian (rad)	1.745 329 X E -2
degree Fahrenheit	degree kelvin (K)	$t_K = (t°f + 459.67)/1.8$
electron volt	joule (J)	1.602 19 X E -19
erg	joule (J)	1.000 000 X E -7
erg/second	watt (W)	1.000 000 X E -7
foot	meter (m)	3.048 000 X E -1
foot-pound-force	joule (J)	1.355 818
gallon (U.S. liquid)	meter^3 (m^3)	3.785 412 X E -3
inch	meter (m)	2.540 000 X E -2
jerk	joule (J)	1.000 000 X E +9
joule/kilogram (J/kg) (radiation dose absorbed)	Gray (Gy)	1.000 000
kilotons	terajoules	4.183
kip (1000 lbf)	newton (N)	4.448 222 X E +3
kip/inch^2 (ksi)	kilo pascal (kPa)	6.894 757 X E +3
ktap	newton-second/m^2 (N-s/m^2)	1.000 000 X E +2
micron	meter (m)	1.000 000 X E -6
mil	meter (m)	2.540 000 X E -5
mile (international)	meter (m)	1.609 344 X E +3
ounce	kilogram (kg)	2.834 952 X E -2
pound-force (lbs avoirdupois)	newton (N)	4.448 222
pound-force inch	newton-meter (N·m)	1.129 848 X E -1
pound-force/inch	newton/meter (N/m)	1.751 268 X E +2
pound-force/foot^2	kilo pascal (kPa)	4.788 026 X E -2
pound-force/inch^2 (psi)	kilo pascal (kPa)	6.894 757
pound-mass (lbm avoirdupois)	kilogram (kg)	4.535 924 X E -1
pound-mass-foot^2 (moment of inertia)	kilogram-meter^2 (kg·m^2)	4.214 011 X E -2
pound-mass/foot^3	kilogram/meter^3 (kg/m^3)	1.601 846 X E +1
rad (radiation dose absorbed)	**Gray (Gy)	1.000 000 X E -2
roentgen	coulomb/kilogram (C/kg)	2.579 760 X E -4
shake	second (s)	1.000 000 X E -8
slug	kilogram (kg)	1.459 390 X E +1
torr (mm Hg, 0° C)	kilo pascal (kPa)	1.333 22 X E -1

*The becquerel (Bq) is the SI unit of radioactivity; 1 Bq = 1 event/s.
**The Gray (Gy) is the SI unit of absorbed radiation.

CONTENTS

ILLUSTRATIONS

TABLES

I INTRODUCTION

This report describes the fabrication processes, the microstructures, and the chemical, physical and mechanical properties of sintered alumina, flame sprayed alumina, plasma sprayed aluminum titanate, plasma sprayed hafnium titanate and plasma sprayed distended beryllium--the materials evaluated in a program to characterize dynamic behavior of porous solids.

II POROUS SINTERED ALUMINA

The porous sintered alumina was underfired WESGO* Al 995 grade powder. The starting material had a mean particle size of 4.2 μm and a maximum particle size of 5.0 μm. The batch number is 3A499, and the nominal composition is

Al_2O_3	99.46
SiO_2	0.20
CaO	0.30
Fe_2O_3	0.02
Na_2O	0.02
TiO_2	trace

Table 1 presents the results of a semiquantitative spectrographic analysis on the starting powder and the crushed porous sintered material. This analysis is typically accurate to ± 50%.

The fabrication cycle consisted of five steps: (1) The powder was made into a slurry and isostatically pressed at room temperature and at 8,000 to 10,000 psi pressure. (2) The compacted agglomerate was green machined, that is, cut up into the desired shapes and rough-ground. (3) The pieces were fired for three hours at a temperature somewhat less than that required to produce dense bodies (underfired). Temperatures of 2800°F, 2400°F, and 2200°F produced bulk porosities of 22%, 36%, and 45%, respectively. (4) The fired pieces were precision-ground by WESGO to make surfaces flat and parallel to within 0.003 inch. (5) The fired pieces were "clean-fired" at 2200°F to remove the machining fluids. The material was furnished as 6 x 9 inch plates of two thicknesses, 1/4 inch and 1/8 inch, and 2-inch-diameter disks, 50 mil thick. All

*Western Gold and Platinum Company, 525 Harbor Blvd., Belmont, California.

Table 1

SPECTROCHEMICAL ANALYSIS OF CERAMIC POWDERS AND POROUS SPECIMENS*

	Al_2O_3			$Al_2O_3 \cdot TiO_2$		$HfO_2 \cdot TiO_2$	
	Sintered 20% porous by Wesgo (%)	Flame spray powder (%)	Flame sprayed on graphite and flaked off (%)	Flame spray powder (%)	Arc-sprayed on graphite and machined off (%)	Spray powder - 200 mesh + 10μ from Cerac (%)	Arc-sprayed on graphite and machined off (%)
Al_2O_3				53.93	53.88		
TiO_2				45.78	45.88	17.6	17.53
HfO_2						81.6	81.24
O_2							19.45
C				0.006			
Li	0.001	<0.001	<0.001	0.004	0.03	<0.03	<0.01
Be	<0.0001	0.0003	0.0002	<0.0002	<0.0002	<0.0001	<0.0001
B	0.0008	<0.0001	0.001	0.001	<0.0006	<0.0001	<0.0003
Na	0.02	>0.1	0.1	0.015	0.03	<0.03	<0.025
Mg	0.2	0.01	0.01	0.06	0.06	0.02	0.025
Al	Major	Major	Major			0.1	0.04
Si	0.15	0.03	0.07	0.02	0.02	0.03	0.015
P	<0.03	<0.03	<0.006	<0.03			
K	0.003	0.003	<0.01	0.006	<0.02		
Ca	0.03	0.02	0.05	0.01	0.01	0.015	<0.008
Ti	0.002	0.02	0.02				
V	<0.0003	<0.0003	<0.0003	<0.002	<0.002	0.007	0.008
Cr	0.002	0.003	0.0018	0.06	0.015	0.003	0.001
Mn	0.0003	0.001	0.001	0.005	0.0015	0.0008	0.0006
Fe	0.03	0.03	0.03	0.06	0.02	0.08	0.03
Co	<0.0003	<0.0003	<0.0005	0.01	0.003	0.007	<0.003
Ni	<0.001	<0.001	0.0005	0.02	0.01	<0.001	<0.001
Cu	<0.001	0.001	0.0001	0.01	0.002	0.003	0.0045
Zu	<0.01	<0.01	<0.003	<0.02	<0.02	<0.01	<0.01
Ga	<0.001	0.02	0.008	0.005	0.006		
Ge	<0.001	<0.001	<0.003	<0.002	0.0006		
As	<0.01	<0.01	<0.002	<0.02			
Rb	<0.01	<0.01	<0.002	0.006	<0.02		
Sr	<0.001	0.001	0.001	0.001	0.0006	<0.01	<0.008
Zr	0.002	0.02	0.05	<0.02	0.001	0.8	1.0
Nb	<0.03	<0.01	<0.01	<0.02	<0.006	<0.025	<0.025
Mo	<0.0003	<0.0003	<0.0003	<0.006	<0.006	<0.0025	<0.0025
Ag	<0.0001	<0.0001	<0.0001	<0.0001	<0.0001	<0.0001	<0.0001
Cd	<0.0003	<0.0003	<0.0003	<0.0002	<0.0006	<0.001	<0.0008
In	<0.0003	<0.0003	<0.001	<0.002	<0.002		
Sn	<0.0003	<0.0003	<0.001	<0.002	<0.006	<0.0025	<0.001
Sb	<0.003	<0.001	<0.003	<0.006	<0.006		
Te	<0.01	<0.01	<0.002	<0.006	<0.02		
Cs	<0.01	<0.01	<0.002	<0.006	<0.06		
Ba	0.001	0.001	0.001	0.005	0.001	<0.0025	<0.008
Ce	<0.03	<0.03	<0.006				
Ta			<0.03		<0.06	<0.3	<0.02
W	<0.01	<0.01	<0.01		0.1		
Tl	<0.001	<0.001	<0.0002	<0.002	<0.006		
Pb	0.002	<0.0003	<0.001	0.005	<0.002	<0.0025	<0.001
Bi	<0.001	<0.0003	<0.001	<0.002	<0.002	0.0025	0.001

* 1. Analyzed by Los Alamos Scientific Laboratory.
2. Numbers are averaged when more than one sample analyzed.

plate and disk surfaces and sample interiors had orange irregular stains, which we identified as iron oxide.* Our attempts at removal were not successful. The semiquantitative spectrographic analysis showed that 0.15 wt% iron oxide was present, whereas the specification called for 0.02 wt%. We concluded that this amount of iron oxide would not affect the impact experiments nor the electron-beam experiments, but that the surface-stained material might be unsuitable for use in underground test experiments because of preferential x-ray absorption.

Figure 1 shows photomicrographs of the grain and pore structures of the three porosity grades. Most grains have smooth, flat sides with rounded edges and corners. There appears to be no preferred orientation and only slight grain growth with increasing firing temperature. Grain sizes for 45%, 36%, and 22% porous material averaged 3, 4, and 5 μm, respectively. Pore sizes averaged about 2 μm for the 22% and 36% porous materials and about 3 μm for the 45% porous material. Pore densities were approximately 2 x 10^4 pores/mm^2 for the higher porosity grades and about $10^4/mm^2$ for the 22% porous material. All materials appeared to be single-phase and free of microcracks. X-ray analyses indicate that the material consisted primarily (99^+ %) of the alpha phase.

Porosimetry measurements were made on sintered 22% porous alumina by Union Carbide Corporation.† The measured pore size distribution (Figure 2) shows the volume-average equivalent pore diameter to be 7 μm with 91% of the pores less than 10 μm. The specific surface area was 0.189 m^2/g.

Tensile strengths and elastic moduli were measured for the three porosity grades by the SRI expanding ring test.[1] Ring specimens of 2.000 ± 0.001 inches ID and 2.500 ± 0.001 inches OD were machined from

---

* Probably from the chuck used to hold the specimens while wet-grinding.

† Nuclear Division, Union Carbide Corporation, P.O. Box Y, Oak Ridge, Tennessee 37830.

1. Sedlacek, R., and F. A. Halden, "Method of Tensile Testing of Brittle Materials," Rev. Sci. Instr. 33, 298 (1962).

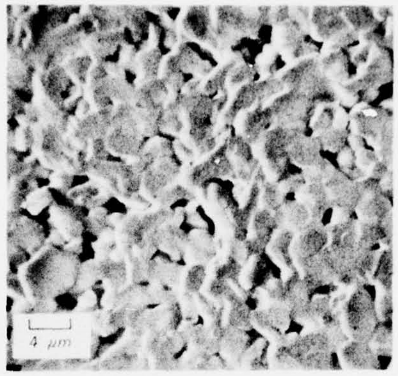

(a) 22% POROUS SINTERED ALUMINA

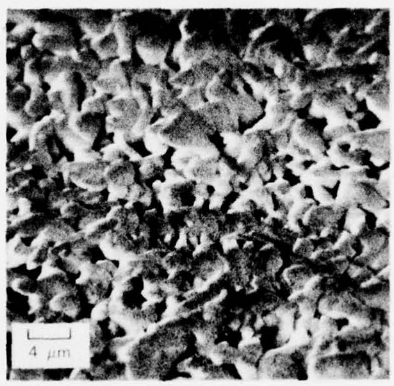

(b) 36% POROUS SINTERED ALUMINA

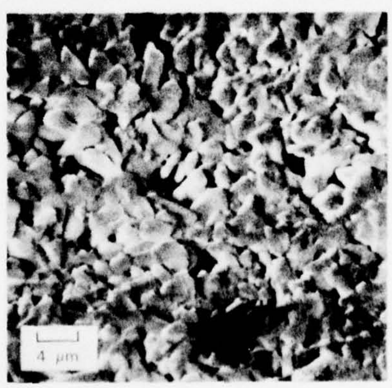

(c) 45% POROUS SINTERED ALUMINA

MP-2407-12

FIGURE 1 SCANNING ELECTRON FRACTOGRAPHS OF 22%, 36%, AND 45% POROUS SINTERED ALUMINA

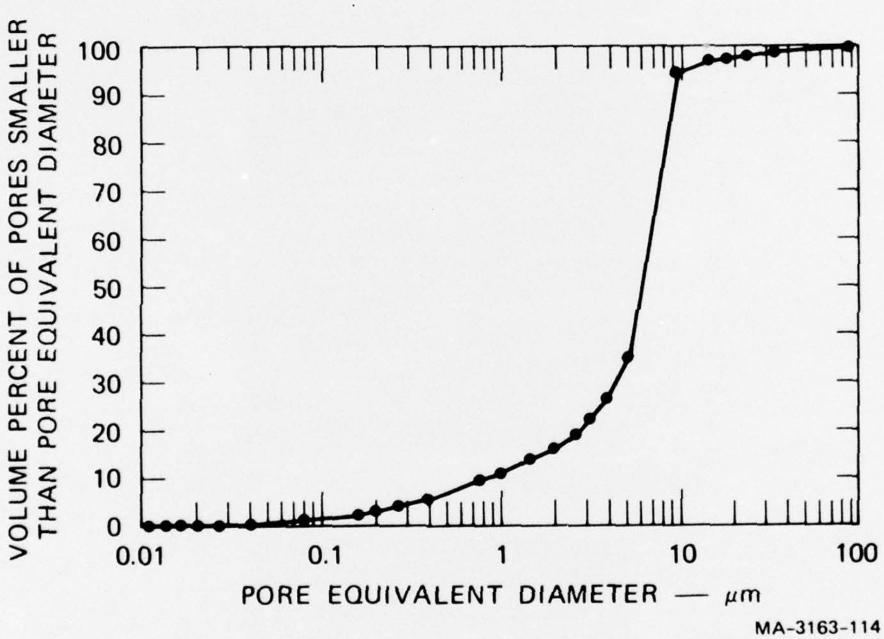

FIGURE 2 PORE SIZE DISTRIBUTION FOR 22% POROUS SINTERED ALUMINA

0.250-inch plates of 22%, 36%, and 45% porous material. A strain gage was cemented to the circumference of each ring, and the specimens were subjected to a monotonically increasing hoop stress at the rate of 3000 psi/min in the test machine.

Hydraulic fluid pressure and resistance change in the strain gage were monitored during each test, and these data were reduced to obtain fracture strengths and moduli. The results are presented in Table 2.

We found evidence of delayed failure (static fagitue) but not of creep. Specimens loaded to, say, 80% of their strength fractured under static load after several seconds. However, there was no perceptible increase in strain during this time.

Table 2

TENSILE PROPERTIES* OF THREE POROSITY GRADES OF SINTERED ALUMINA

Percent Porosity	Specimen Number	Fracture Strength (ksi)	Young's Modulus (ksi x 10^3)
22%	1	19.4	32.8
	2	21.1	30.0
36%	1	11.6	14.5
	2	9.2	14.8
45%	1	3.2	5.82
	2	3.5	5.57

* Measured with the SRI expanded ring test.

Longitudinal and transverse sound speeds were measured on flat disk samples by the pulse echo technique and the results used to estimate Poisson's ratio and Young's modulus (see Table 3). The acoustic values of Young's modulus are in reasonable agreement with the vales from mechanical tests (Table 2).

The affinity of water vapor in the atmosphere to adsorb on surfaces of Al_2O_3 is well known, and the presence of liquids in pores has been shown to affect the shock response of materials significantly.[2] Therefore, we performed simple weight loss experiments to determine the amount of water adsorbed on exterior and interior surfaces. Samples of 22%, 36%, and 45% porous Al_2O_3, held at 500°C for 1½ hours, equilibrated in a desiccator, and then weighed, indicated less than 0.01 wt% adsorbed water. More sophisticated thermal gravimetric analyses confirmed this result.

---

2. Murri, W. J., "Shock Compression and Release of Mechanical Mixtures of Water and Porous Earth Materials, J. Appl. Mech., 42, 395-398, (1975).

Table 3

ACOUSTICAL PROPERTIES OF THREE POROSITY GRADES OF WESGO AL 995 SINTERED ALUMINA

Porosity	Longitudinal Sound Speed C_ℓ(mm/µsec)	Transverse Sound Speed C_s(mm/µsec)	Density, ρ g/cm^3	Poisson's Ratio,* ν	Estimate of Young's Modulus,† E(ksi)
22%	9.22	5.63	3.16	0.20	35.0×10^3
36%	7.13	4.39	2.6	0.19	17.4×10^3
45%	5.61	2.96	2.2	0.31	7.31×10^3

* $\nu = [(C_\ell/C_s)^2 - 2]/[2(C_\ell/C_s)^2 - 2]$

† $E = \left\{[(1 - 2\nu)(1 + \nu)]/(1 - \nu)\right\} \cdot C_\ell^2 \rho$

III FLAME-SPRAYED ALUMINA

Approximately 225 free-standing, flame-sprayed alumina samples 50 to 100 mils thick were manufactured by LASL for SRI. The starting powder was Metco Al_2O_3-99 grade* with mean and mode particle sizes of 30.7 μm and 18.5 μm, respectively. Spectrochemical analysis is given in Table 1.

Alumina powder was flame-sprayed onto a roughened graphite substrate with a Metco 5P Thermo-spray gun operated at 22 psi oxygen and 14 psi acetylene pressure and mounted at a standoff distance of $5\frac{1}{2}$ inches, traversing the substrate at a constant speed of 19 feet per minute.

The alumina coating, when built up to the desired thickness by making a number of passes, was removed, cored into disks or sliced into squares, and diamond-ground to dimension.

Figure 3a shows a photomicrograph of a polished cross section of a flame-sprayed alumina disk. The layering texture and the elongated grains are in sharp contrast with the microstructure of sintered material, Figure 1. Average grain size of the flame sprayed material was about 10 μm, or about one-third the mean particle size of the sprayed powder. The pores are five to ten times smaller than those in the 22% porous sintered material, but flame-sprayed alumina appears to have five to ten times as many pores. The pores appear to be of two types: those located at the intersections of the elongated grains, and those located within grains and probably arising from vaporization of overheated droplets. The porosimetry results on a flame sprayed sample are shown in Figure 4 for comparison with Figure 2. The specific surface area was 0.403 m^2/g and the volume-average equivalent pore diameter was 0.94 μm, with 98% of the pores less than 10 μm in diameter.

---

*Metco, Inc., 1105 Prospect Avenue, Westbury, N.Y.

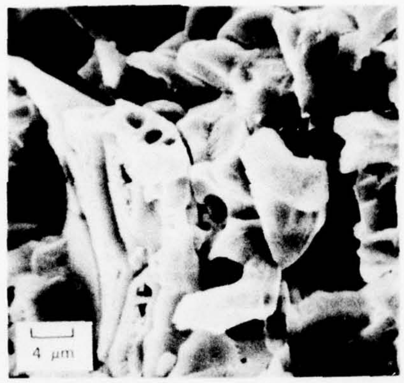

(a) FLAME-SPRAYED ALUMINA

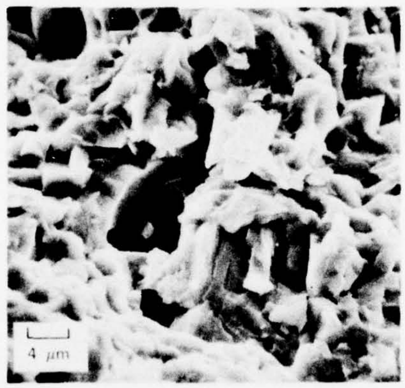

(b) PLASMA-SPRAYED ALUMINUM TITANATE

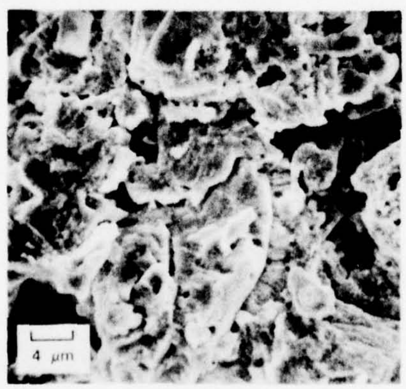

(c) PLASMA-SPRAYED HAFNIUM TITANATE

MP-2407-13

FIGURE 3 SCANNING ELECTRON FRACTOGRAPHS OF (a) FLAME-SPRAYED ALUMINA, (b) PLASMA-SPRAYED ALUMINUM TITANATE, AND (c) PLASMA-SPRAYED HAFNIUM TITANATE

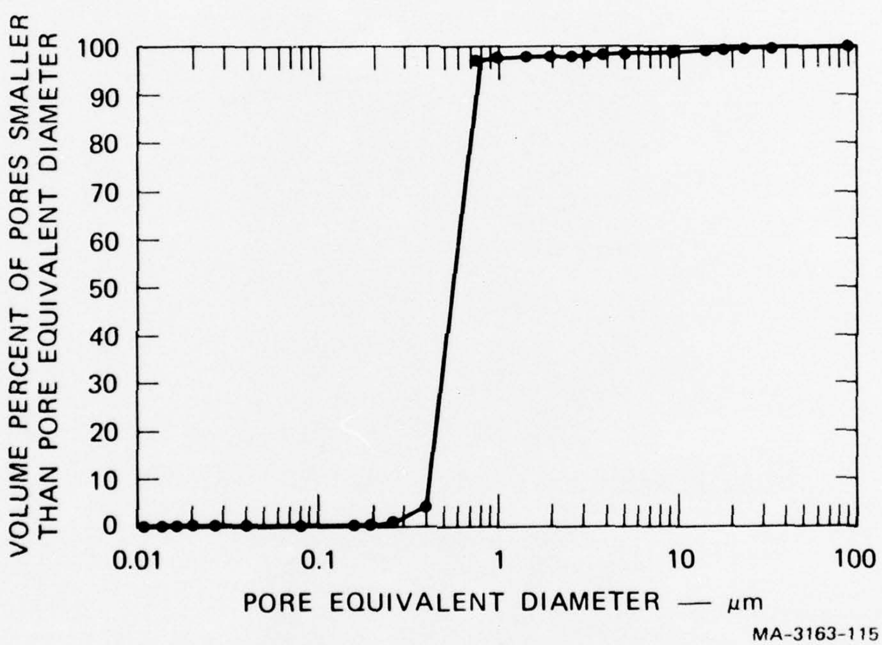

FIGURE 4 PORE SIZE DISTRIBUTION FOR FLAME-SPRAYED 22% POROUS ALUMINA

IV PLASMA-SPRAYED ALUMINUM TITANATE

The spectrochemical analysis and the particle-size distribution of the Al_2TiO_5 starting powder are given in Table 1 and Figure 5, respectively. The powder consisted of 53.9% Al_2O_3 (by difference), 45.7% TiO_2, and 60 ppm carbon. The average particle size was 16.9 ± 7.2 μm; the mean and the mode were 17.7 and 15.5 μm, respectively. Specific surface area was 0.163 m^2/g. X-ray examination showed the powder to consist principally of β-$Al_2O_3 \cdot TiO_2$ (tielite) with one or more impurity phases of insufficient quantity to permit identification. The approximate parameters of the titanate were a ≃ 3.60 Å, b ≃ 9.48 Å, and c ≃ 9.67 Å.

The Al_2TiO_5 powder was sprayed onto roughened and cleaned graphite plates using a Plasmadyne SG-1B plasma spray gun at a standoff distance of 3 inches and an arc-power setting of 400 A. Other spraying parameters are given in Table 4. When the coating on the 11½-inch x 11½-inch graphite plate was built up to 0.080-0.095 mils thickness, the coating was removed, cut into 1½-inch squares and diamond-ground dry using glue to hold the squares to a plate. The ground squares were then cleaned with acetone.

Figure 3b is a photomicrograph of a fractured cross section showing the layered microstructure. The flattened grains show a preferred texture in the spraying direction, an indication that the powder melted fully in the plasma arc and was quenched upon deposition, causing columnar grains to grow outward from the graphite substrate. The frequent cracks observed in the coating were probably produced by thermal stresses during solidification and cooling.

Average grain size was about 6 μm. Porosimetry data were not available. The mean density and longitudinal sound speed were 3.38 g/cm^3 and 0.386 cm/μs, respectively.

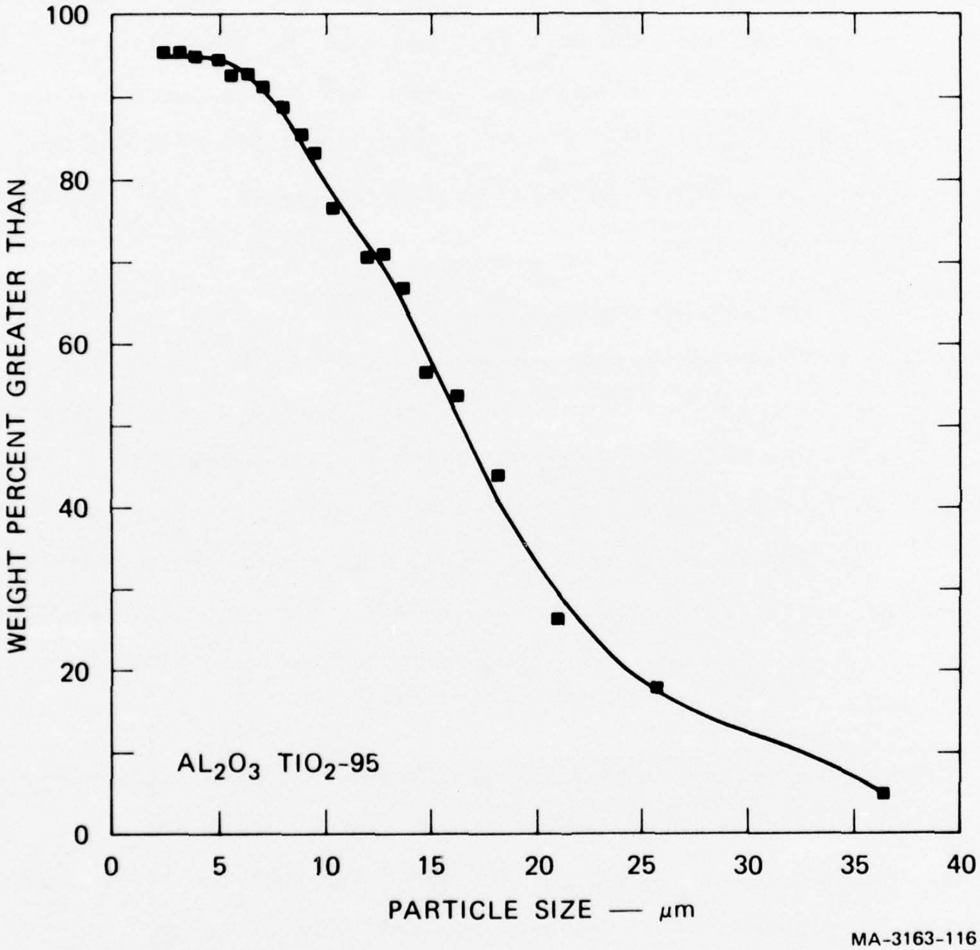

FIGURE 5 CUMULATIVE PARTICLE SIZE DISTRIBUTION OF ALUMINUM TITANATE POWDER USED IN PLASMA SPRAYING

Table 4

SPRAYING PARAMETERS FOR ALUMINUM TITANATE AND HAFNIUM TITANATE

	Aluminum Titanate	Hafnium Titanate
Arc-gas pressure	50 psi	50 psi
Arc-gas flow	45 CFH	50 CFH
Carrier gas pressure	30 psi	55 psi
Carrier gas flow	15 CFH	15 CFH
Arc-power setting	400A	300A
Feed screw speed setting	Feeder #2, 150	Feeder #1, 16-1/2
Cannister vibrator setting	75%	75%
Part-to-gun distance	3 in.	3-1/4 in.
Cooling air	40 psi	40 psi

X-ray diffractometer examination by LASL of the flame-sprayed alumina coatings showed that both α and γ alumina were present. Furthermore, the relative amounts of the two phases were found to be about equal. The α phase was present as unusually large crystallites, whereas the γ phase was present in more finely crystalline form, as evidenced by particle-size broadening. The different γ peak intensities were essentially orientation-independent.

V PLASMA-SPRAYED HAFNIUM TITANATE

The spectrochemical analysis and the particle size distribution of the hafnium titanate starting powder are given in Table 1 and Figure 6, respectively. The powder consisted of 81.6% HfO_2, 17.6% TiO_2, and about 0.8% Zr. Average particle size was 30.2 ± 11.6 μm; the mean and the mode particle sizes were 27.0 μm and 2.5 μm, respectively. Specific surface area was 0.158 m^2/g. Two major phases were identified using x-ray techniques. The intended orthorhombic hafnium titanate with approximate parameters a = 5.18 Å, b ≃ 5.07 Å, and c ≃ 5.62 Å made up 40 to 50% of the total weight. The remainder was a monoclinic boddeleyite-type phase with approximate parameters a ≃ 5.04 Å, b ≃ 5.17 Å, c ≃ 5.18 Å, and $\beta \simeq 99^\circ$, most likely a $(Hf,Ti)O_2$ solid solution phase.

As was done for the aluminum titanate material, the hafnium titanate powder was sprayed onto roughened and cleaned graphite plates $11\frac{1}{2}$ x $11\frac{1}{2}$ inches square using a Plasmadyne SG-1B spray gun. The spraying parameters are given in Table 4, for comparison with those used for the aluminum titanate powder. Approximately one hundred squares about 1.5 inches on a side were cut while still adhered to the graphite substrate. After removal from the substrate, the squares were diamond-ground on a surface grinder using no grinding fluid. These squares required no cleaning after grinding.

The photomicrograph in Figure 3c of a fractured cross section shows a structure apparently less layered than for the aluminum titanate. The more equiaxed grain shapes and the angular voids between grains indicate that the hafnium titanate did not achieve the same degree of melting as the aluminum titanate. The transgranular microcrack shown in the figure is evidence of thermal cracking. Average grain size was about 8 μm. Porosimetry experiments were not performed. Mean density

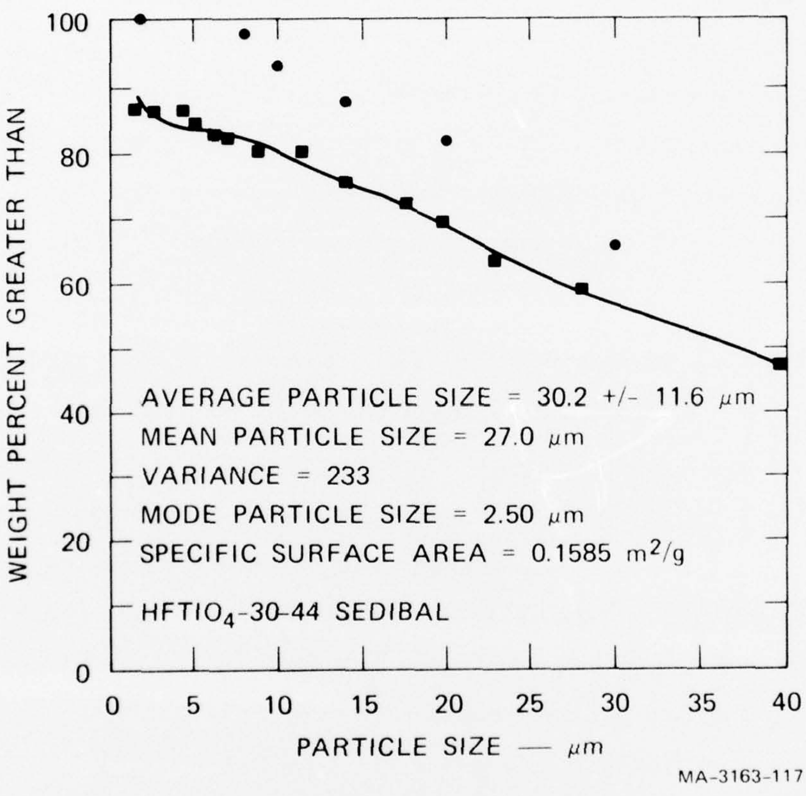

FIGURE 6 CUMULATIVE PARTICLE SIZE DISTRIBUTION OF HAFNIUM TITANATE POWDER USED IN PLASMA SPRAYING

and longitudinal sound speeds were 6.97 g/cm^3 and 0.298 cm/μs, respectively. X-ray diffraction studies of the sprayed material showed no significant differences in the diffraction patterns. The relative line intensities of the two phases changed somewhat, indicating that the relative percentage of the orthorhombic phase had decreased, perhaps as a result of some loss of oxygen.

VI SPRAYED POROUS CERAMICS ON 3DQP SUBSTRATES

Twelve disks of three-dimensionally reinforced quartz phenolic fiber composite (3DQP) were spray-coated with porous ceramics by LASL. The 1.5-inch-diameter, 0.15-inch thick disks were charred freehand before coating using a Plasmadyne SG-1B (S1-AS version) plasma spray gun operating at 500 A, 50 psi argon pressure, 50 ft^3/hr argon flow, at a standoff distance of about 2 inches.

Eight specimens were flame-coated with alumina, two were plasma coated with aluminum titanate, and two were plasma coated with hafnium titanate. The specimens were held on a water-coated vacuum chuck that traversed back and forth in front of the spray gun at a rate of 19 feet per minute. The standoff distance was fixed at 5½ inches. All other parameters were as described in Table 4 for freestanding ceramic specimens. Table 5 provides a summary of the results. These specimens were not used during the course of this program, but the material characterization data is presented in anticipation of their possible future use.

Table 5

SPRAY-COATED THREE-DIMENSIONALLY REINFORCED QUARTZ PHENOLIC

Sample*	Coating Material	Wt after Charring (g)	Wt after Coating (g)	Coating Wt (g)	Sample Thickness (in.)	Coated Thickness (in.)	Coating Thickness (in.)
24	Alumina	7.247	8.028	0.781	0.155	0.165	0.010
25	"	7.473	8.177	0.704	0.158	0.168	0.010
26	"	7.407	8.110	0.703	0.159	0.169	0.010
27	"	7.492	8.158	0.666	0.158	0.168	0.010
28	"	7.286	8.019	0.733	0.158	0.168	0.010
29	"	7.374	8.067	0.693	0.158	0.168	0.010
30	"	7.370	8.173	0.803	0.157	0.167	0.010
31	"	7.382	8.093	0.711	0.157	0.167	0.010
32	Aluminum titanate	7.365	8.173	0.810	0.157	0.167	0.010
33	" "	7.514	8.565	1.051	0.158	0.169	0.011
34	Hafnium titanate	7.408	8.811	1.403	0.157	0.167	0.010
35	" "	7.493	9.035	1.542	0.157	0.167	0.010

*1.5-in. diam., 0.15-inch thickness.

VII PLASMA-SPRAYED DISTENDED BERYLLIUM (PSDB)

Porous beryllium plasma sprayed disks 14-3/4 inches in diameter with a $2\frac{1}{2}$-inch diameter hole in the center were obtained in two thicknesses, 0.09-inch and 0.18-inch, from Union Carbide Corporation, Indianapolis, Indiana.

The starting powder used in spraying these disks, KBI* Lot No. 0843, was produced from a high purity ($>$ 99%) beryllium by an impact attrition process (also called cold streaming) which yields a more equiaxed particle rather than the sheet-like particles in high purity electron flake powders. More than 90% of the particles had diameters between 10 μm and 44 μm; the chemical analyses is given in Table 6.

Four disks were fabricated by plasma-spraying the beryllium powder onto an aluminum substrate to approximately twice the finished thickness. Each beryllium disk was then mechanically removed from the substrate and sawed into five equal radial segments. The density of each disk was determined by sawing off a portion of each segment and measuring the density according to ASTM B-328. Each segment was then ground flat and parallel to the appropriate dimensions using a 60-grit alumina grinding wheel with deionized water as the coolant on a once-through basis. Following grinding, the segments were dewatered in a vacuum furnace heated to $300^{\circ}C$. Pumping and heating was continued until the vacuum was better than 10^{-5} torr. The furnace was then cooled and backfilled with argon. The parts were removed and immediately sealed in plastic bags. All segments were of 85 $\pm$ 0.5% theoretical density ($1.85\ g/cm^3 = 100\%$). Figure 7 shows pore size distribution as measured by mercury porosimetry. Table 6 gives a chemical analysis of one of the segments.

---

*Kawecki Berylco Industries, Inc., P.O. Box 429, Hazelton, PA 18201.

Table 6

CHEMICAL ANALYSIS OF STARTING POWDER AND PLASMA-SPRAYED BERYLLIUM DISKS‡

	Starting Powder	Plasma-Sprayed Disk
Be Assay	99.17	98.42
BeO	0.75	1.60
C*	0.057	0.112
Fe†	0.113	0.118
Aℓ	0.039	0.058
Mg	0.045	0.029
Ni	0.015	0.015
Mn	0.009	0.010
Cr	0.008	0.014
Ca	--	0.020
Co	--	0.0005
Cu	0.007	0.009
Zn	--	< 0.010
Ag	--	0.0008
Pb	--	0.0001
Si	0.020	0.023
Mo	--	< 0.001
Ti	0.017	0.011

*By Leco

†By wet chemistry.

‡By Kawecki Berylco

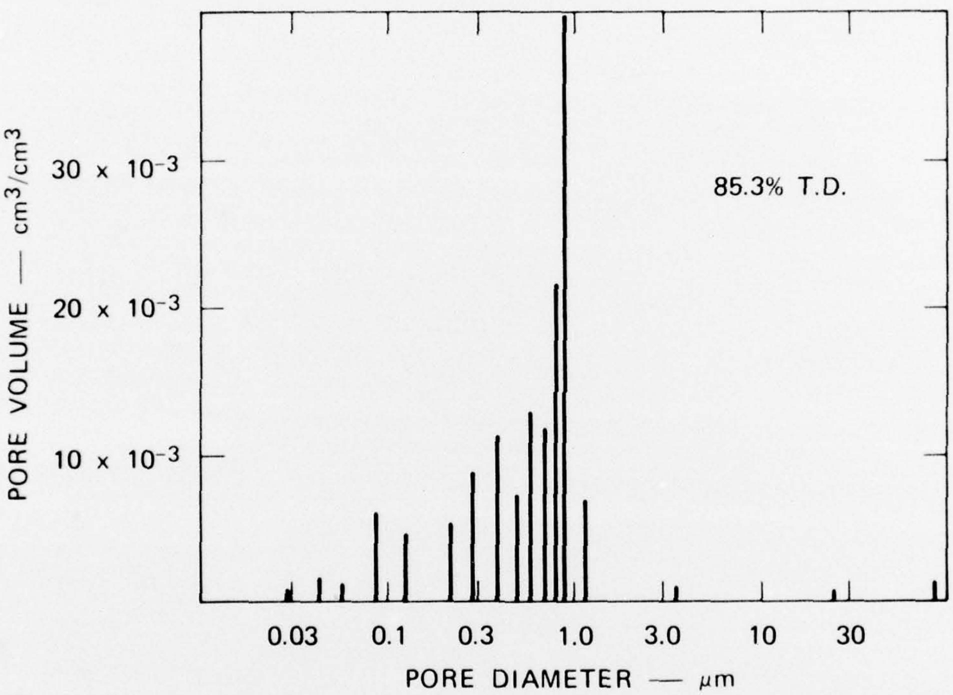

*Union Carbide Corporation

MA-3163-118

FIGURE 7 TYPICAL PORE SIZE DISTRIBUTION BY MERCURY POROSIMETRY IN PLASMA-SPRAYED BERYLLIUM SAMPLES OF 85% THEORETICAL DENSITY*

The microstructure of the beryllium disks (Figure 8) was revealed by viewing polished and etched cross sections of the disks in an optical microscope. The dominant characteristics are the elongated grains and the numerous pores. Grain size and pore size distributions were not quantitatively determined.

PSDB specimens used in electron-beam experiments were examined metallographically after irradiation. The surface layers of the plates were found to have a distinctly different appearance from the interior, and a distinct boundary existed about 225 μm below the surface, Figure 9. This led us to question whether the mechanical and acoustical properties of the surface differ from those of the interior. The grains in the surface regions were large and elongated, typical of plasma-sprayed material, but the structure in the interior was not discernible on unetched specimens. Etching in 15% HF, however, showed that the interior also consisted of elongated grains, Figure 10, so that the microstructure appeared uniform. Hence, we conclude that glue used to hold slabs of beryllium together at the gage planes has an etching effect on beryllium, and that no variation in microstructure or mechanical properties occurs through the specimen thickness.

(a) BRIGHT FIELD ILLUMINATION

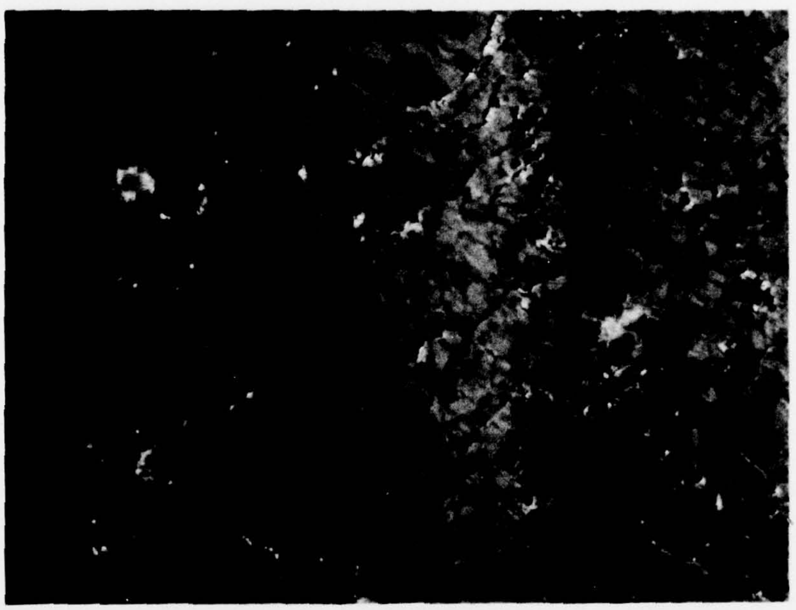

(b) POLARIZED LIGHT

MP-3163-3

FIGURE 8 MICROSTRUCTURE OF PSDB (UNETCHED)

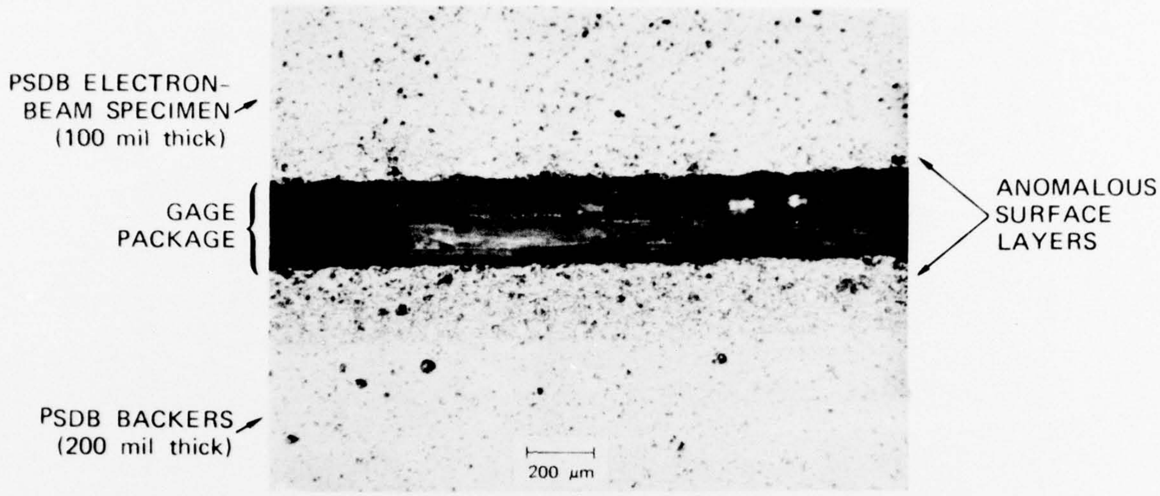

(a) ELECTRON-BEAM EXPERIMENT 4

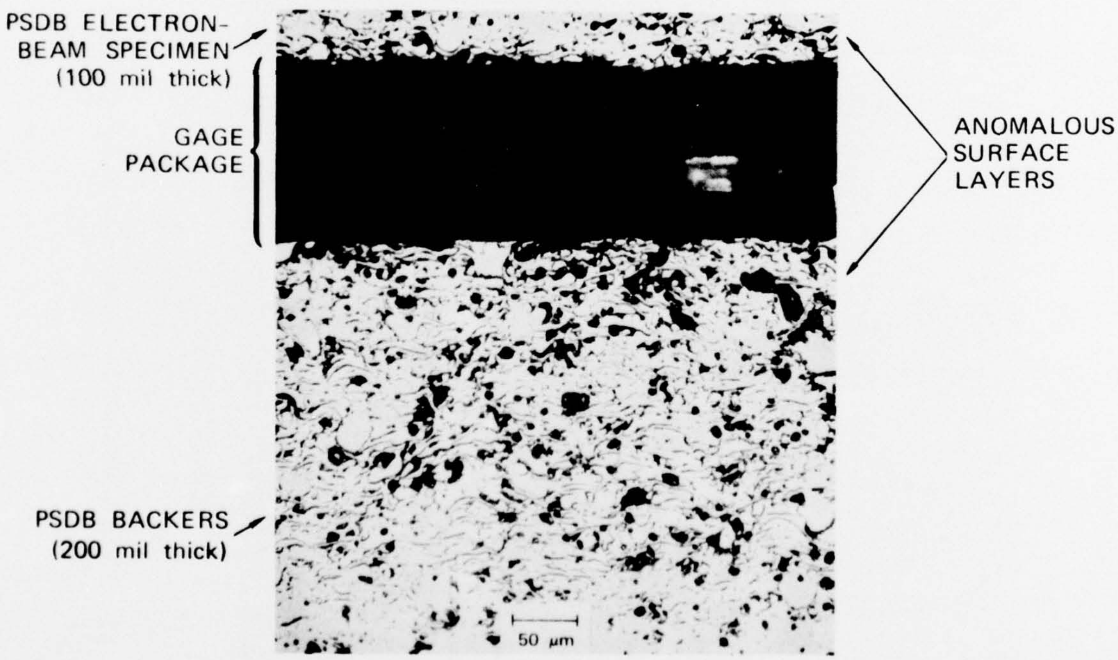

(b) ELECTRON-BEAM EXPERIMENT 2

MP-3163-4

FIGURE 9 POLISHED CROSS SECTIONS OF TWO ELECTRON-BEAM IRRADIATED SPECIMENS OF PSDB SHOWING ANOMALOUS SURFACE LAYERS (ELECTRON-BEAM DIRECTION WAS FROM TOP TO BOTTOM)

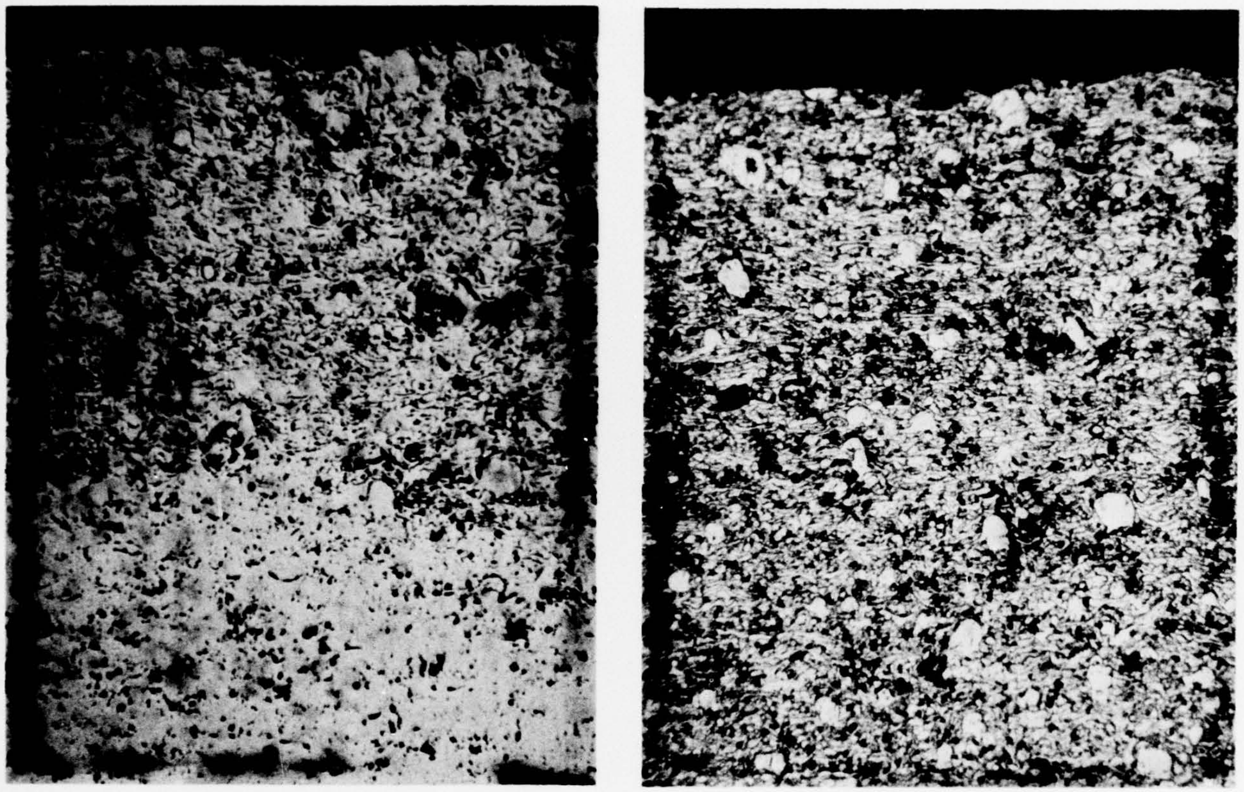

(a) UNETCHED

(b) ETCHED

MP-3163-5

FIGURE 10 CROSS SECTIONS OF BERYLLIUM SPECIMEN SHOWING THE MICROSTRUCTURE NEAR THE SURFACE

DISTRIBUTION LIST

DEPARTMENT OF DEFENSE

Director
Defense Advanced Rsch. Proj. Agency
ATTN: Strategic Tech. Office

Defense Communication Engineer Center
ATTN: Code 720, John Worthington

Director
Defense Communications Agency
ATTN: NMCSSC, Code 510

Defense Documentation Center
12 cy ATTN: TC

Director
Defense Intelligence Agency
ATTN: DI-7D
ATTN: DT-1C, Nuc. Eng. Br.
ATTN: DT-2, Wpns. & Sys. Div.

Director
Defense Nuclear Agency
ATTN: STSI, Archives
ATTN: DDST
ATTN: STSP
3 cy ATTN: STTL, Tech. Lib.
3 cy ATTN: SPAS

Dir. of Defense Rsch. & Engineering
ATTN: DD/S&SS
ATTN: AD/OS
ATTN: AD/DS

Commander
Field Command
Defense Nuclear Agency
ATTN: FCTMOF
ATTN: FCPR
ATTN: FCTMD

Director
Joint Strat. Tgt. Planning Staff, JCS
ATTN: JLTW-2
ATTN: JPTM
ATTN: JPTP

Chief
Livermore Division, Fld. Command DNA
Lawrence Livermore Laboratory
ATTN: FCPRL

OJCS/J-5
ATTN: J-5, Plans & Policy, R&D Div.

DEPARTMENT OF THE ARMY

Program Manager
BMD Program Office
ATTN: DACS-BMZ
ATTN: DACS-BMT, John Shea
ATTN: DACS-BMZ-D, Julian Davidson
ATTN: DACS-BMT, Clifford E. McLain

DEPARTMENT OF THE ARMY (Continued)

Commander
BMD System Command
ATTN: BDMSC-TEN, Noah J. Hurst

Dep. Chief of Staff for Rsch., Dev. & Acq.
ATTN: NCB Division

Deputy Chief of Staff for Ops. & Plans
ATTN: Dir. of Chem. & Nuc. Ops.

Commander
Harry Diamond Laboratories
ATTN: DRXDO-RC, Robert B. Oswald, Jr.
ATTN: DRXDO-NP
ATTN: DRXDO-RBH, James H. Gwaltney

Commander
Picatinny Arsenal
ATTN: SMUPA-MD, Henry Opat
ATTN: SARPA-ND-C-T, Donald Miller
ATTN: SARPA-FR-E, Louis Avrami

Commander
TRASANA
ATTN: R. E. DeKinder, Jr.

Director
U.S. Army Ballistic Research Labs.
ATTN: Robert E. Eichelberger
ATTN: DRXBR-TB, J. T. Frasier
ATTN: DRXRD-BVL, William J. Schuman, Jr.

Commander
U.S. Army Mat. & Mechanics Rsch. Ctr.
ATTN: DRXMR-HH, John F. Dignam

Commander
U.S. Army Materiel Dev. & Readiness Cmd.
ATTN: DRCDE-D, Lawrence Flynn

Commander
U.S. Army Missile Command
ATTN: DRSMI-XS, Chief Scientist
ATTN: DRSMI-RRR, Bud Gibson
ATTN: DRS-RKP, W. B. Thomas
ATTN: DRCPM-PE-EA, Wallace O. Wagner

Commander
U.S. Army Nuclear Agency
ATTN: ATCA-NAW

DEPARTMENT OF THE NAVY

Chief of Naval Material
ATTN: MAT 0323, Irving Jaffe

Chief of Naval Operations
ATTN: OP-985D
ATTN: OP-62
ATTN: OP-985

Chief of Naval Research
ATTN: Code 464, Thomas P. Quinn

DEPARTMENT OF DEFENSE CONTRACTORS (Continued)

Institute for Defense Analyses
ATTN: Joel Bengston
ATTN: IDA, Librarian, Ruth S. Smith

Ion Physics Corporation
ATTN: Robert D. Evans

Kaman AviDyne
Division of Kaman Sciences Corp.
ATTN: Norman P. Hobbs

Kaman Sciences Corporation
ATTN: Albert P. Bridges
ATTN: Thomas Meagher
ATTN: Frank H. Shelton
ATTN: Jerry L. Harper
ATTN: John R. Hoffman

Lockheed Missiles & Space Company
ATTN: A. P. Hardt
ATTN: Lloyd F. Chase
ATTN: Raymond R. Capiaux
ATTN: F. G. Borgardt

Martin Marietta Aerospace
Orlando Division
ATTN: Laird Kinnaird

McDonnell Douglas Corporation
ATTN: L. Cohen
ATTN: J. Kirby
ATTN: J. F. Garibotti
ATTN: R. J. Reck

National Academy of Sciences
ATTN: National Materials Advisory Board for
Donald G. Groves

Northrop Corporation
ATTN: Don Hicks

Physics International Company
ATTN: Doc. Con. for James Shea

Prototype Development Associates, Inc.
ATTN: John Slaughter

R & D Associates
ATTN: Albert L. Latter
ATTN: Jerry Carpenter
ATTN: Harold L. Brode
ATTN: F. A. Field

Science Applications, Inc.
ATTN: R. Fisher
ATTN: G. Ray

DEPARTMENT OF DEFENSE CONTRACTORS (Continued)

Science Applications, Inc.
ATTN: J. Courtney

Southern Research Institute
ATTN: C. D. Pear

Stanford Research Institute
ATTN: Donald Curran
ATTN: Herbert E. Lindberg
ATTN: George R. Abrahamson
ATTN: Donald A. Shockey
ATTN: M. J. Ginsberg
ATTN: A. B. Lutze
ATTN: J. P. Wilhelm

Stanford Research Institute
ATTN: Harold Carey

Systems, Science & Software, Inc.
ATTN: G. A. Gurtman
ATTN: Russell E. Duff

Terra Tek, Inc.
ATTN: Sidney Green

DEPARTMENT OF THE NAVY (Continued)

Director
Naval Research Laboratory
ATTN: Gerald Cooperstein, Code 7770
ATTN: Mario A. Persechino, Code 5180
ATTN: Tech. Lib., Code 2027

Commander
Naval Sea Systems Command
ATTN: 0333A, Marlin A. Kinna

Commander
Naval Surface Weapons Center
ATTN: W. Carson Lyons, Code 323
ATTN: Navy Nuc. Prgms. Off., Code WA-501
ATTN: Leo F. Gowen, Code 2302

Director
Strategic Systems Project Office
ATTN: NSP-272, CDR Leslie Stoessl

DEPARTMENT OF THE AIR FORCE

AF Materials Laboratory, AFSC
ATTN: MAS
ATTN: MBC, Donald L. Schmidt
ATTN: T. Nicholas

AF Rocket Propulsion Laboratory, AFSC
ATTN: RTSN, G. A. Beale

AF Weapons Laboratory, AFSC
ATTN: SUL
ATTN: DYS, Lt E. J. Burns
ATTN: DYV
ATTN: Dr. Minge

Commander
Foreign Technology Division, AFSC
ATTN: TDFBD, J. D. Pumphrey
ATTN: TDPTN

HQ USAF/RD
ATTN: RDPM
ATTN: RDQ
ATTN: RDQSM
ATTN: RD
ATTN: RDQPN

SAMSO/DY
ATTN: DYS

SAMSO/MN
ATTN: MNNR

SAMSO/RS
ATTN: RSSE
ATTN: RSS

Commander in Chief
Strategic Air Command
ATTN: DOXT
ATTN: XPFS

ENERGY RESEARCH & DEVELOPMENT ADMINISTRATION

Division of Military Application
ATTN: Doc. Con. for Res. & Dev. Br.
ATTN: Doc. Con. for CDR Richard E. Peterson
ATTN: Doc. Con. for
Lieutenant Colonel Donald L. McNutt

ENERGY RESEARCH & DEVELOPMENT ADMINISTRATION (Continued)

University of California
Lawrence Livermore Laboratory
ATTN: C. Joseph Taylor, L-92
ATTN: Joseph E. Keller, Jr., L-125
ATTN: G. Staihle, L-24

Los Alamos Scientific Laboratory
ATTN: Doc. Con. for J. W. Taylor
ATTN: Doc. Con. for John McQueen
ATTN: Doc. Con. for R. S. Thurston

Sandia Laboratories
Livermore Laboratory
ATTN: Raymond Ng
ATTN: Doc. Con. for T. Gold
ATTN: Doc. Con. for C. S. Hoyle
ATTN: Doc. Con. for 8131, H. F. Norris, Jr.

Sandia Laboratories
ATTN: Doc. Con. for Albert Chabai
ATTN: Doc. Con. for R. R. Boade
ATTN: Doc. Con. for D. McCloskey

DEPARTMENT OF DEFENSE CONTRACTORS

Aeronautical Rsch. Assoc. of Princeton, Inc.
ATTN: Coleman Donaldson

Aeronutronic Ford Corporation
Aerospace & Communications Ops.
ATTN: P. Spangler

Aerospace Corporation
ATTN: W. Barry
ATTN: R. Allen
ATTN: Richard Crolius, A2, Rm. 1027

Avco Research & Systems Group
ATTN: John Gilmore, E-502
ATTN: John E. Stevens, E-500

Battelle Memorial Institute
ATTN: Merwyn R. Vanderlind
ATTN: W. Pfeifer

The Boeing Company
ATTN: Brian Lempriere

Brown Engineering Company, Inc.
ATTN: Ronald Patrick

Effects Technology, Inc.
ATTN: Robert Wengler

General Electric Company
Space Division
ATTN: G. Harrison
ATTN: Carl Anderson
ATTN: Phillip Cline, Rm. 3700

General Electric Company
TEMPO-Center for Advanced Studies
ATTN: DASIAC

General Research Corporation
ATTN: Robert E. Rosenthal